RESEARCH PAPER

Flexible microspectrometer for grape maturation monitoring in the vineyard

Sophie Jenne,[a,*] Alessio Tugnolo,[b] Hugo M. Oliveira,[c] and Hans Zappe[a]
[a]University of Freiburg, Laboratory for Micro-optics, Department of Microsystems Engineering, Freiburg, Germany
[b]Università degli Studi di Milano, Department of Agricultural and Environmental Sciences, Milan, Italy
[c]International Iberian Nanotechnology Laboratory, Braga, Portugal

ABSTRACT. Optical spectroscopy is a well-suited technique for the nondestructive and real-time maturation monitoring of fruits and vegetables. Although many commercial spectroscopy systems exist, including some for portable use in the field, a significant gap in agricultural monitoring is the ability to continuously measure the condition of fruits in the field over longer periods of time. To this end, we present here a fully integrated, flexible microspectrometer consisting of multiple light sources and multiple broadband photodiodes for the spectral evaluation of grape maturation in the field. To enable the microspectrometer design, a customized grape berry model generated from the optical properties, primarily light scattering, of grape berries was developed. The microspectrometer was fabricated using a scalable fabrication process based on a spin-coated, flexible polyimide substrate. Experiments were conducted both in a controlled laboratory environment as well as during the grape maturation period in the vineyard and these demonstrated that the spectral properties of grapes at different maturation stages can be accurately measured. Using suitable chemometric models, the amount of total soluble solids in °Br, which is the most important factor for the maturation estimation of grapes, was determined from the microspectrometer data.

1 Introduction

In modern viticulture, the quality control of grapes is crucial for the production of high-quality wines. The currently most common and reliable technique for the maturation assessment of grapes is based on wet-chemical analysis of grape composition in the laboratory. However, the reliability of this established method is limited by the number of sample grape berries picked in the vineyard, and there is usually a considerable time delay (often 1 day or more) between sampling and knowledge of the results, such that the point of optimal ripeness can easily be missed. In addition, laboratory-based chemical analysis requires skilled operators for the measurements and can generate a considerable amount of chemical waste.[1]

The use of visible/near-infrared spectroscopy for the evaluation of the ripeness of grapes, measuring parameters, such as soluble solids, total acidity, and total phenols,[2–7] can overcome these limitations. Eliminating labor-intensive and time-consuming analyses of the collected fruit

---

*Address all correspondence to Sophie Jenne, sophie.jenne@imtek.uni-freiburg.de

samples not only can lower the costs for the analysis but also has significant environmental advantages compared to traditional methods.

Such spectroscopic approaches based on reflectance[8] or fluorescence[9] for grape ripeness assessment exist, but these are based on bulky devices that would need to be adapted to be suitable for the monitoring of the fruit composition in the vineyard. Examples include the Multiplex 3, manufactured by Force-A, and the SpectraPen, both of which assess reflectance and fluorescence at specific wavelengths to determine the amount of soluble solids, pH, as well as anthocyanin and flavonol content.[7,10] However, these systems are not suitable for continuous grape maturation monitoring in the field, as they are large handheld pieces of equipment that require skilled operators to execute the measurements. Furthermore, in the context of large vineyards, obtaining comprehensive information on the overall crop maturation status would necessitate a large number of measurements at numerous locations, which can be a time-consuming, and thus expensive, process. To address these issues, one promising approach for a less bulky and less expensive spectroscopic sensor able to determine the maturation status of grapes has been proposed by Pampuri et al.[11] This prototype uses two commercially available six-channel integrated spectrometers operating in the VIS and NIR wavelength regions. Despite the considerable reduction in the size of the spectrometer, the entire device is still large and cannot be embedded into a grape bunch for continuous monitoring.

As a result of these known limitations, we can state that a spectroscopic sensor suitable for continuous monitoring of the maturation of grapes in the vineyard would need to fulfill the following requirements: highly miniaturized overall system dimensions, allowing placement of the sensor inside a grape bunch without causing damage to the fruit and without interfering in the ripening process; the ability to acquire continuous time-resolved data; robustness with respect to the environment in the field; and an overall simplicity and low cost, permitting a large number of sensors to be deployed thereby also enabling spatially resolved (in the vineyard) data acquisition.

Based on these demands, we present here a compact visible/near-infrared spectrometer designed to monitor grape maturation in a continuous and autonomous manner suitable for deployment in the field. Operating in reflection mode, the microspectrometer was designed to be placed inside a grape bunch at the beginning of the maturation period and continuously measure the grape maturation throughout the maturation period, a time scale of weeks to months. We show here how this standalone device can overcome the drawbacks of current maturation assessment techniques.

2 Microspectrometer Design

As illustrated in the sketch of the system design shown in Fig. 1(a), the microspectrometer was designed to be placed inside the grape bunch during the maturation period and removed before harvesting. It is placed in such a way that the berries grow around the microspectrometer.

The boundary conditions for the design of the microspectrometer were given by the geometry of the grape bunch. Typically, spectrometers detect light that has interacted with a sample under investigation either in reflection or transmission mode. In both cases, light emitted from suitable light sources interacts with the sample, where it is either absorbed, scattered, or reflected and detected by the photodiodes. For the application presented in this work, the reflectance mode was employed, as in this mode light sources and detectors can be placed on the same side of the sample, which is advantageous considering its use in the field.

Furthermore, as the microspectrometer should not cause bruises to the grape berries or cause fouling due to water accumulation on the device, the microspectrometer was manufactured on a flexible substrate and highly miniaturized; it can thus follow the shape of the grape berries in the bunch. As seen in Fig. 1(a), the driving and control electronics needed to operate the microspectrometer were separated from the microspectrometer canopy and placed outside of the grape bunch, at the cane of the vine plant. The microspectrometer strip itself only comprised the light sources and detectors and was placed inside the bunch.

To ensure a high flexibility of the microspectrometer strip, it was fabricated based on a flexible polyimide circuit board; the detailed fabrication process is described in Sec. 4. Figure 1(b) shows the schematic layout of the sensing head located at the end of the microspectrometer strip. Four LED light sources, emitting the four peak wavelengths 530, 635, 685, and
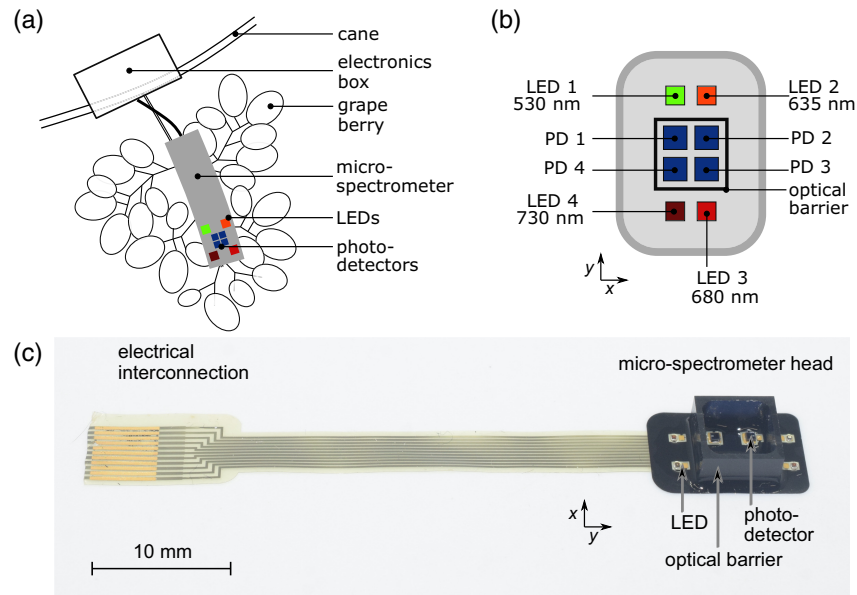
Fig. 1 (a) Schematic illustration of the microspectrometer system as deployed in the field. The driving and control electronics are placed outside the grape bunch, at the cane or poles next to the plant. The flexible microspectrometer itself, with the light sources and detectors, is located inside the grape bunch. (b) Layout of the microspectrometer head at the end of the flexible strip, containing four LEDs (LED 1 to LED 4) and four photodiodes (PD 1 to PD 4). The light sources and detectors are separated by an opaque barrier to minimize optical crosstalk. The center-to-center distance of the LEDs and the closest photodetector is 3.25 mm in y direction and 0 mm in x direction. The center-to-center distance of the photodetectors is 2.8 mm. (c) Photograph of the microspectrometer: The microspectrometer head comprises the LEDs and photodiodes, which are optically separated by an optical barrier. An electrical connector allows electrical interconnection with the control electronics. Since the microspectrometer head consists of rigid chips and a rigid optical barrier, this part, in contrast to the rest of the microspectrometer, is not flexible.

730 nm, and broadband photodiodes were employed. The particular wavelengths of the LEDs were chosen based on the previous research,[12–14] since spectral changes at these wavelengths well represent changes in the chemical composition during the maturation process. In particular, changes around 530, 680, and 635 nm are associated with changes in chlorophyll concentration. During the maturation, chlorophyll degrades as sugars and anthoxyanins are created. Additionally, spectral changes around 740 nm are caused by the third overtone of –OH bond stretching and therefore indicate the presence of water and sugars. The emitters and detectors were separated by an opaque barrier to eliminate stray light reaching the detectors without interaction with the sample.

A photograph of the microspectrometer with a total length of 5.6 cm is shown in Fig. 1(c). It can be divided into two parts, the electronic interface on the one side and the spectrometer unit on the other side. The four LEDs are placed on the outer side of the optical barrier, and the photodetectors are placed on the inside of the barrier. The microspectrometer head was covered with an (IrO_x/Ir/IrO_x) multilayer, which is highly optically absorbing and therefore reduces stray light. The dimensions of the microspectrometer head are 12 mm in the y direction and 8 mm in the x direction.

3 Optical Simulations

To understand the basics of light interaction between the microspectrometer and grape berries, optical ray-tracing simulations were performed using OpticStudio (Zemax LLC.). To have an accurate representation of a grape berry, an optical model was generated as detailed in Sec. 3.1. The primary influencing parameters impacting the spectroscopic reading are identified and characterized in Sec. 3.2.

3.1 Realistic Grape Berry Model

To enable a comprehensive analysis of the interaction between the microspectrometer and the grape, a model of a grape berry was established; a comprehensive description of this procedure can be found in prior publications.[15,16] In summary, the optical properties, namely the absorption and scattering coefficients, μ_a and μ_s, respectively, and the scattering anisotropy factor g were determined for the pulp and peel of three table grape cultivars (ARRA 15/white-green, Tawny Seedless/red, and Melody Blagratwo/black). The absorption and scattering coefficients were computed from spectroscopic raw data utilizing the inverse adding doubling method,[17,18] a model widely used for scattering and absorbing samples with arbitrary thickness.

Based on these values, three-dimensional grape berry models were generated within OpticStudio to facilitate the development of the microspectrometer. For the optical simulations, the nonsequential mode was utilized, and the Henyey–Greenstein distribution was employed to model the bulk scattering within the grape berries.

The Henyey–Greenstein function $p(\cos\theta)$ provides a mathematical representation of the directional distribution of light that is scattered by submicron particles. It is commonly expressed as the summation of its constituent components, resulting in the following equation:

$$p(\cos\theta) = \frac{1 - g^2}{2 \cdot (1 + g^2 - 2 \cdot g \cdot \cos\theta)^{\frac{3}{2}}},$$ (1)

with θ being the deflection angle of a photon after a scattering event and g, the anisotropy factor, is also expressed as the cosine expectation[19] of θ, i.e.,

$$g = \int_0^\pi p(\theta)\cos\theta \cdot 2\pi\sin\theta d\theta.$$ (2)

The input parameters required for the Henyey–Greenstein model in OpticStudio comprise the optical mean free path mfp, which represents the distance that a photon traverses within a medium before it is either absorbed or scattered. The mean free path can be expressed as a function of the absorbing and scattering coefficients[19] simply as

$$mfp = \frac{1}{\mu_a + \mu_s}.$$ (3)

Using this model, the light propagation inside the grape berry and at the air/berry interface of the white-green grape cultivar ARRA 15 was first studied. The berries were represented by two prolate spheroids, as illustrated in Fig. 2(a). The first spheroid, used to model the grape peel, exhibited a longitudinal axis length of $a_1 = 29.91$ mm and a transverse axis length of $a_2 = 19.70$ mm. A second spheroid, having an identical origin but possessing reduced axis lengths, was utilized to mimic the pulp tissue. The current study subtracted a peel thickness of 189 μm[15] from the axis length of the second spheroid, thereby producing the inside of the grape berry. This resulted in a grape model that thus consists of a pulp spheroid surrounded by a layer of fruit peel.
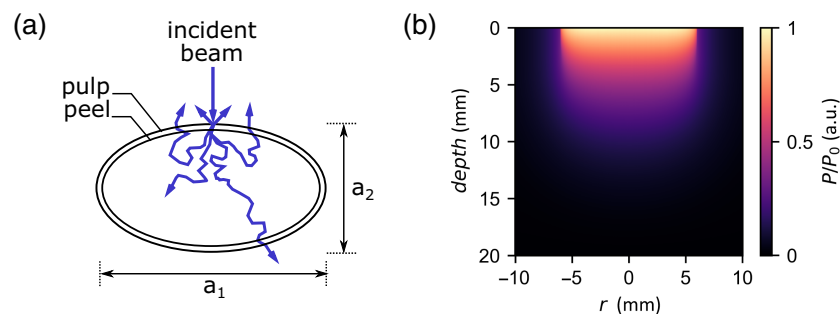

Fig. 2 (a) Schematic illustration of the grape berry model. Two spheroids represented the pulp and the peel of the berry. Light incident into the grape is either reflected at the air/berry interface or penetrates into the fruit where scattering and/or absorption occur. (b) Color map representing the light distribution inside the grape berry in terms of detected power (in a.u.) at each point. It is clearly seen that forward scattering dominates the behavior.
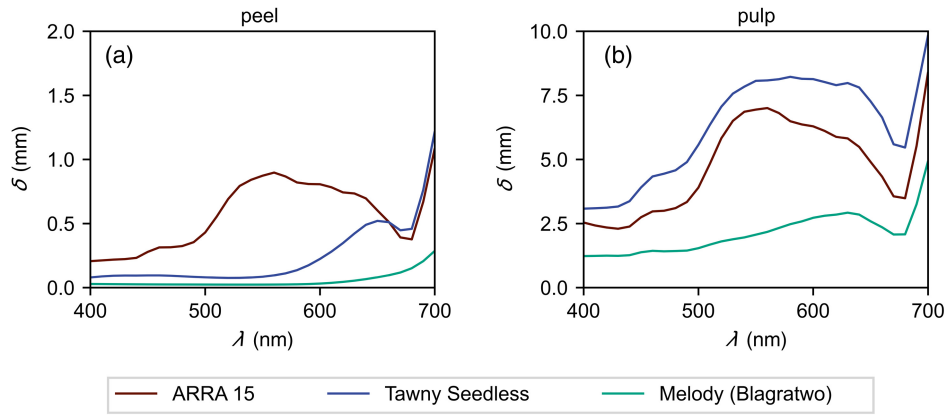
Fig. 3 Penetration depth of light at wavelengths ranging from 400 to 700 nm for the (a) peel and (b) pulp of the three different grape varieties ARRA 15 (white/green), Tawny Seedless (red) and Melody (black). Generally, the penetration depth is smaller in the peel of the grape berries compared to the pulp and the darkest grape variety. Melody has the lowest penetration depths of light into both, the peel and the pulp.

To study the light propagation and inside the grape berry, the power detected at distinct depths within the fruit was recorded. Figure 2(b) shows a color map representing the light distribution inside a grape berry. As light enters the fruit, the detected intensity decreased in the direction of and perpendicular to the propagation direction. However, forward scattering was identified as the prevailing scattering mechanism resulting in a slower power decay in the direction of penetration compared to the radial direction. The positive value of the scattering anisotropy coefficient ($g > 0$) of grape berries and flesh confirms this observation.

The quantification of the decay of light intensity inside the grape berry was also performed by investigating the penetration depth, denoted as δ. Specifically, the penetration depth indicates the depth at which the intensity degradation reaches a value of 37% ($1/e$) from its initial value and may be written as[20]

$$\delta = \frac{1}{\sqrt{3\mu_a \cdot (\mu_a + \mu_s(1 - g))}}.$$ (4)

The findings of the light penetration depth into the peel and pulp of ARRA15, Tawny, and Melody grape berries at wavelengths ranging from 400 to 700 nm are presented in Fig. 3. In addition, Table 1 provides a summary of the optical properties and resulting penetration depths for $\lambda = 530$ nm. The depth of penetration for all grape cultivars analyzed was significantly higher in the pulp [Fig. 3(b)] than in the peel [Fig. 3(a)]. When comparing between grape varieties,

Table 1 Optical properties of the pulp of Arra 15 (white/green), Tawny Seedless (red), and Melody Blagratwo (black) berries at 530 nm. From the absorption and scattering coefficients, μ_a and μ_s, and the anisotropy factor g, the penetration depths of light into the berries' peel and pulp can be derived.

Grape variety	μ_a (mm^{-1})	μ_s (mm^{-1})	g	δ (mm)
ARRA 15, peel	5.74×10^{-1}	19.11	0.989	0.79
ARRA 15, pulp	4.48×10^{-2}	2.146	0.939	6.51
Tawny Seedless, peel	6.5	20.55	0.889	0.07
Tawny Seedless, pulp	3.97×10^{-2}	2.096	0.949	7.57
Melody Blagratwo, peel	22.4	21.822	0.781	0.02
Melody Blagratwo, pulp	2.25×10^{-2}	2.797	0.932	1.89

it was observed that darker varieties possessed a lower penetration depth, while lighter cultivars had a comparatively higher penetration depth. Furthermore, the peel of Tawny and Melody Blagratwo exhibited a penetration depth within the range of the peel's thickness, thereby resulting in lower transmission of light to the underlying pulp tissues. For all grape varieties, less scattering and absorption were observed in the pulp when compared to the peel, resulting in increased depths of penetration.

3.2 Characterization of Influencing Parameters

After studying the general light interaction with grapes, optical simulations were conducted to study the impact of the microspectrometer position with respect to the grape berry. The impact of the distance and tilt of the microspectrometer with respect to the grape berries are detailed in the following.

3.2.1 *Distance*

The findings from the optical simulations indicate a significant variation in the detected signal intensity as a function of the distance between the microspectrometer and grape berry. According to the findings depicted in Fig. 4, there is a quadratic decay in the detected signal power as the distance between the grape and photodiodes increases. It is noteworthy that when the distance between the microspectrometer barrier and the grape surface is 0 mm, the microspectrometer and grape berry are in contact.

3.2.2 *Tilt*

Furthermore, as illustrated in Fig. 4(b), a significant decrease in the total detected power was observed as the degree of tilt between the microspectrometer and the grape increases. The term "tilt" in this context pertains to the angular difference between the normal vector of the microspectrometer plane and the normal vector of the horizontal plane along the longitudinal axis of the grape berry. As the degree of tilt increased from a starting value of 0 deg, where the plane of the microspectrometer is parallel to the grape berry, the detected power decreased until beyond a 60 deg tilt angle, no reflected signal was detected. Beyond 60 deg, reflected light is absorbed by the opaque barrier separating light sources and detectors.
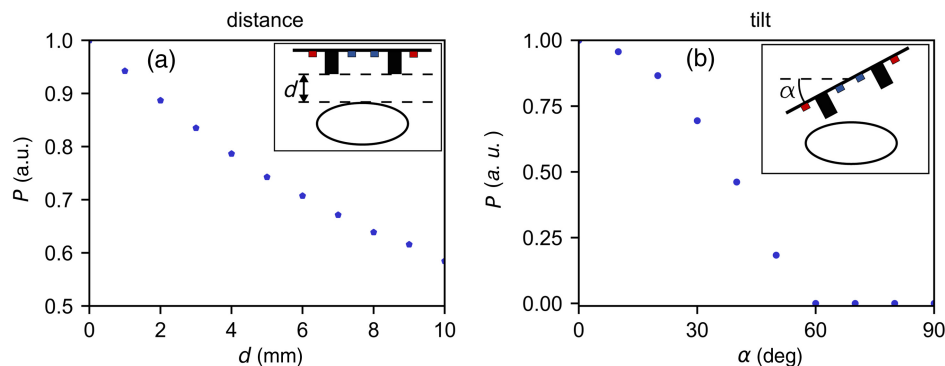

Fig. 4 Normalized power of the detected signal depending on the distance and tilt between microspectrometer and grape berry. As distance and tilt increase, the detected signal decreases. For the determination of the influence of the distance, the tilt was kept constant at $\alpha = 0$ deg, and when the tilt is varied, the distance was kept constant at 6 mm. The values are normalized to the highest value measured. For the distance, the power was normalized to the power measured at $d = 0$ mm and for the tilt, the power was normalized to the power measured at $\alpha = 0$ deg. The schematic sketches illustrate the geometrical arrangement of the microspectrometer and the grape berry. In the cross-sectional view of the microspectrometer, the LEDs are shown in red, the photodetectors in blue, and the optical barrier is black.

3.2.3 *Conclusions for in-field application*

For the implementation of the microspectrometer in the grape bunch, the presented data indicate that the placement of the microspectrometer demands adherence to two essential criteria: first, the microspectrometer tilt with respect to the sample should be kept at an absolute minimum; and second, the microspectrometer's distance from the grape berries should be as close as possible to allow the detection of maximum power, thereby enhancing the signal-to-noise ratio.

4 Microspectrometer Fabrication

The fabrication of the microspectrometers used a 4-in. silicon handle wafer and the process steps illustrated in Fig. 5.

Referring to the numbering in Fig. 5, the process begins with (1) a layer of polyimide (U-Varnish-S, UBE) with a thickness of 5 μm spun onto a silicon handle wafer and cured in a nitrogen atmosphere at a temperature of 450°C for 10 min. Polyimide is highly suited as a base material for the flexible microspectrometer because of its high flexibility, mechanical strength, and especially its excellent chemical resistance.[21,22] Subsequently, (2) 50 nm of gold was sputtered onto the polyimide base layer to create electrical wiring with a width of 200 μm, which was afterward structured by lift off. 5 nm of chromium and 50 nm of platinum served as adhesion promoters for the gold layer. In a second spin-coating step, (3) a 5 μm polyimide top layer was applied to encapsulate the electric circuit, followed by another curing at 450°C for 10 min.

Subsequently, (4) all contact pads were opened by reactive ion etching of the second polyimide layer. Within this step, the outlines of the microspectrometers were also etched. After that, (5) 500 nm gold was electroplated onto the contact pads, using 3 μm chromium as an adhesion promoter. Then (6) a multilayered iridium oxide and iridium composite (400 nm IrO$_x$/200 nm Ir/400 nm IrO$_x$) was sputtered to act as an absorption layer and reduce the internal and external stray light. Next, (7) the microspectrometer stripes were delaminated from the silicon handle wafer, (8) and (9) the optoelectronic components were placed onto the microspectrometer stripe by attaching the bottom contacts of the dies with conductive glue, and (10) the top contacts were electrically connected using ball-wedge bonding with a 30 μm wire. The LEDs used were the C527EZ290 (green, width × length × height = $280 \times 280 \times 170\ \mu$m^3, Cree); C4L-H12T5 (orange, $313 \times 313 \times 190\ \mu$m^3, Chips4Light); C4L-R12T5 (red, $313 \times 313 \times 190\ \mu$m^3, Chips4Light); and LA CI13WP3 (infrared, $330 \times 330 \times 190\ \mu$m^3, Light Avenue). The detector was LA-PD32HP1 ($800 \times 800 \times 220\ \mu$m^3, Light Avenue). (11) The LEDs and photodetectors
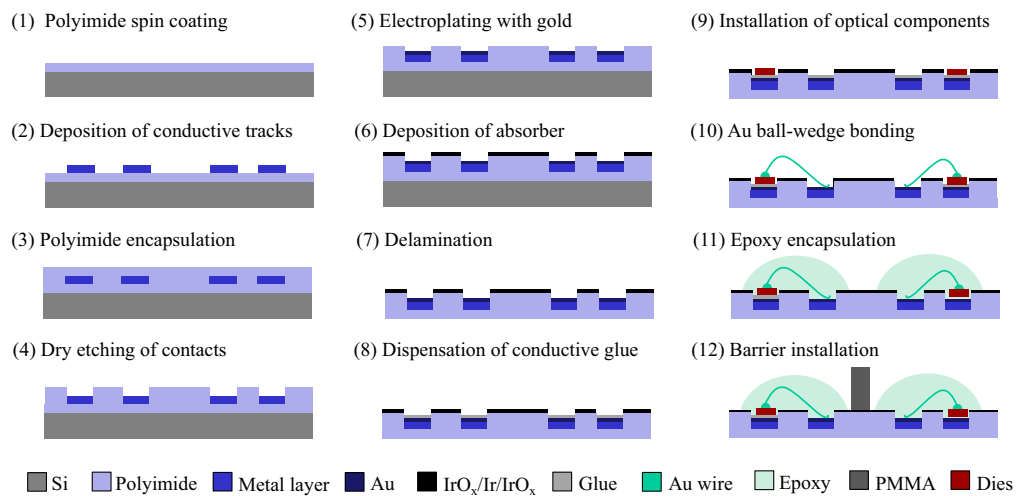

Fig. 5 Schematic illustration of the microfabrication process for the flexible microspectrometers. Polyimide is spun on a silicon handle wafer and the conductive tracks are sputtered. A second polyimide layer encapsulated the circuitry and contacts were opened with dry etching. After delamination, the optoelectronic components were installed, encapsulated and an optical barrier separated the light sources and detectors.

were then encapsulated using an optical epoxy (EPO-TEK 302-3M, Epoxy Technology) to protect the gold bonds and the light sources and detectors from environmental influences in the final application.

To reduce optical crosstalk arising from light reaching the photodetectors without interaction with the sample, (12) an optical barrier CNC-milled from nontransmissive poly(methyl methacrylate) with an edge width of 6 mm and a height of 3 mm was installed between light sources and detectors. Finally, the contact end of the microspectrometer stripe was thickened with two layers of polyimide tape. Thus the microspectrometer can be connected to the driving and control electronics using flexible printed circuit connectors. The electronics module in the main consisted of an eight-channel LED driver, analog-to-digital converter, and a transimpedance amplifier and is described in detail elsewhere.[1]

5 Maturation Monitoring

The thus-fabricated microspectrometers were first characterized in the laboratory and subsequently employed for measurements in the field.

5.1 Spectra at Different Maturation Stages

To characterize the performance of the microspectrometer under controlled and ideal boundary conditions, the spectra of grapes at three different maturation stages were acquired in the laboratory. Therefore, 20 grape berries of the grape variety pinot noir were collected in the field at three distinct phases in grape ripening: (a) at the end of the fruit development, i.e., when the berries were still green; (b) at veraison, which is the point at which the grape berries start to change their color; and (c) when the berries were ripe for harvesting.

As a reference, the spectra in a range of 500 to 800 nm were first acquired using a commercial tabletop UV/VIS spectrometer (UV-3600i Plus, Shimadzu) together with an integrating sphere (ISR-1503, Shimadzu). The integrating sphere collected all specular reflectance occurring at the grape surface and the light re-emitted from the grape sample.

For the analysis with the microspectrometer, the same berries were placed in contact with the optical barrier of the microspectrometer, and the tilt of the microspectrometer with respect to the transverse axis of the berries was fixed at 0 deg. For each grape berry, one measurement was performed. In total, measurements of 60 different grape berries were undertaken, where 20 berries were examined for each maturation stage.

To allow a comparison of the data acquired with the commercial spectrometer, the flexible microspectrometer was calibrated using a two-point calibration of the photodiodes before the spectrum acquisition, in which the minimum and maximum readout values of the photodiodes were determined for 0% and 100% reflection, respectively. For the minimum reflectance values, the LEDs were turned on sequentially, while the photodiodes were covered, resulting in the minimum readout values arising from the photodiode's dark current. In contrast, for 100% reflection, the readout maximum was determined by measuring the maximum reflection of a barium sulfate ($BaSO_4$) standard white plate.

The resulting spectra of the grape berries at the three different maturation stages acquired with the commercial spectrometer and the microspectrometer are summarized in Fig. 6. Clearly, the spectra change as the maturation advances and the detected reflectance decreases for the wavelength range under investigation. The largest changes were observed in the visible region, around 530 to 550 nm, arising from the green to purple/black color change of the grape peel and the superficial pulp during maturation.[23] This color change results from the degradation of chlorophyll[24,25] and is enhanced by the accumulation of anthocyanins in these fruit parts.

Although the data points acquired with the microspectrometer were shifted to slightly lower values when compared to the data from the commercial spectrometer, they follow the spectral reflectance features caused by the change of the chemical composition throughout the maturation period. Furthermore, higher inhomogeneities in the maturation stage of the different grape berries under investigation resulted in higher standard deviations of the acquired data of the commercial spectrometer as well as of the microspectrometer.
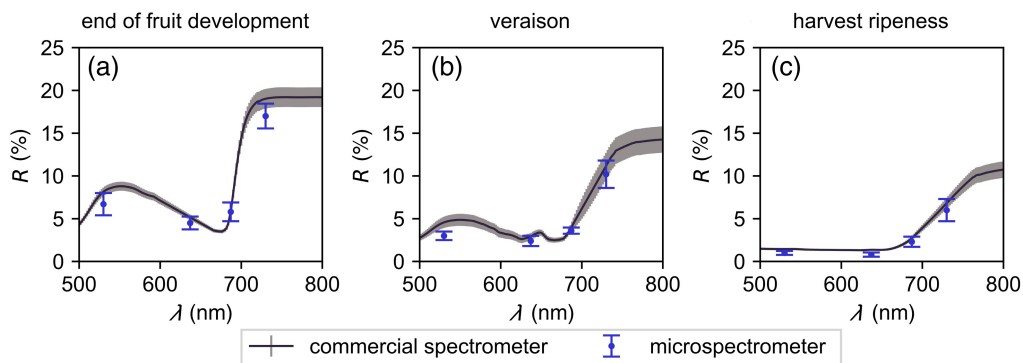
Fig. 6 Reflectance spectra of grape berries at three different maturation stages acquired with a commercial spectrometer and the microspectrometer as the maturation process advances from (a) the end of the fruit development to (b) the veraison and (c) harvest ripeness. Each data point presents the mean reflectance data ± standard deviation measured for 20 different berries at the three different maturation stages. In total, 60 different berries were investigated.

5.2 In-Field Maturation Monitoring

Finally, the microspectrometer was used for maturation monitoring evaluated in a grape vineyard during one maturation season. In this trial, five microspectrometers were placed in a vineyard cultivated with pinot noir grapes, located at the Kaiserstuhl, Baden, Germany. Measurements were performed on a semi-weekly basis, each time after sunset.

Photographs of the microspectrometer inside a grape bunch at veraison, when deployed in the field and close to harvest ripeness are shown in Fig. 7. As seen in Fig. 7(a), the electronics box was mounted on a pole and the microspectrometer was placed inside the bunch in such a way that the grape berries surround the measurement head. Figure 7(b) shows a photograph of the microspectrometer and the grape bunch at veraison, and Fig. 7(c) closes to harvest ripeness, showing that no undesired movements of the microspectrometer occurred while it was deployed in the field, and the grape berries were not damaged. In contrast to the laboratory experiments presented earlier, the field experiments started at veraison and not at the end of the fruit development.

The acquired data from one of the microspectrometers placed in the field are shown in Fig. 8. For each LED, the reflected signal was acquired at each of the photodetectors. Similar to the experiments performed in the laboratory, it is seen that at NIR wavelengths a higher reflection is detected as compared to visible wavelengths.
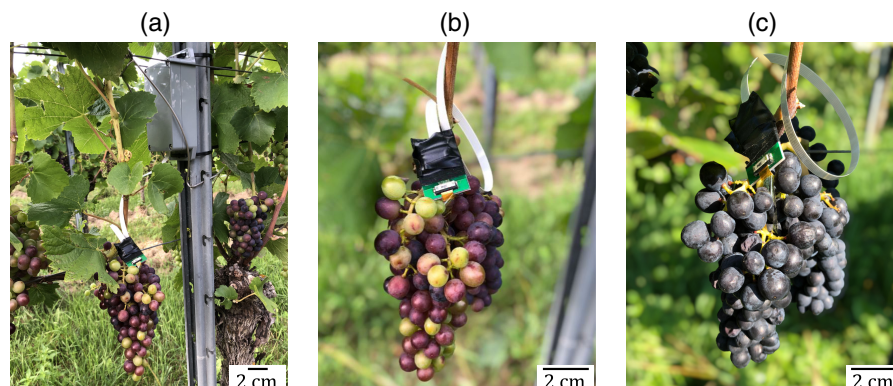

Fig. 7 Photographs of the microspectrometer placed in the vineyard. (a) The microspectrometer is deployed at veraison. The electronics box is mounted on a pole and the microspectrometer placed inside the grape bunch. Therefore, the microspectrometer head is not visible in the photo; (b) detailed picture of the microspectrometer inside the grape bunch at veraison; and (c) close to harvest ripeness. The microspectrometer head is clamped between two adjacent grape berries, which prevent the movement of the microspectrometer during the measurement period. It is in contact with the grape berry. Five microspectrometers each stayed in the field for 3 weeks.
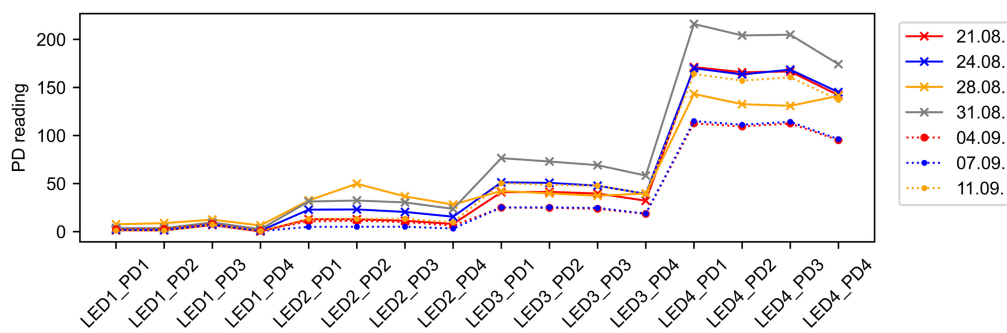
Fig. 8 Spectroscopic reading from one microspectrometer placed in the vineyard. For each of the four LEDs, the reflectance was measured at all four photodetectors (hence 16 measurements). Applying a PLS model to these values results in the TSSs concentrations shown in Fig. 9.

The spectral raw data were then correlated to the amount of total soluble solids (TSS) in degrees Brix (°Bx) using the partial least squares (PLS) model described elsewhere.[1] 1°Bx corresponds to 1 g of sucrose dissolved in 100 g of solution, i.e., grape juice.

As a reference, after each measurement series, 20 different grape berries from the same part of the vineyard were picked and mashed. The berries were not picked from the grape bunches which were investigated with the microspectrometer, but from grape bunches located close to these. The refractive index n_D of the grape juice was determined at 20°C at the D-line ($\lambda = 589$ nm) using a commercial refractometer (SCHMIDT + HAENSCH GmbH & Co). The refractive index was then correlated with the °Bx value according to the International Commission for Uniform Methods of Sugar Analysis (ICUMSA) table [26] using the polynomial fit:

$$°\text{Bx} = 11758.74 \times n_D^5 - 88885.21 \cdot n_D^4 + 270177.93 \times n_D^3 - 413145.80 \times n_D^2$$
$$+ 318417.95 \times n_D - 99127.4536. \tag{5}$$

The ICUMSA table contains a set of standardized values that correlate Brix and refractive index measurements of sugar solutions and is used in industry as a uniform method for measuring sugar content in solutions using refractometry.

The results of the reference measurements are summarized in Fig. 9(a). During the observation period, the refractive index increased continuously from 1.35947 to 1.36336, and the TSS from 17.32 to 19.69°Bx, values measured on August 21, 2023 and September 11, 2023, respectively. The values obtained from the microspectrometer correlate closely with this data: TSS increases from 16.98 ± 1.35°Bx at veraison to 19.54 ± 0.51°Bx close to harvest ripeness. The correlation coefficient is 0.82.
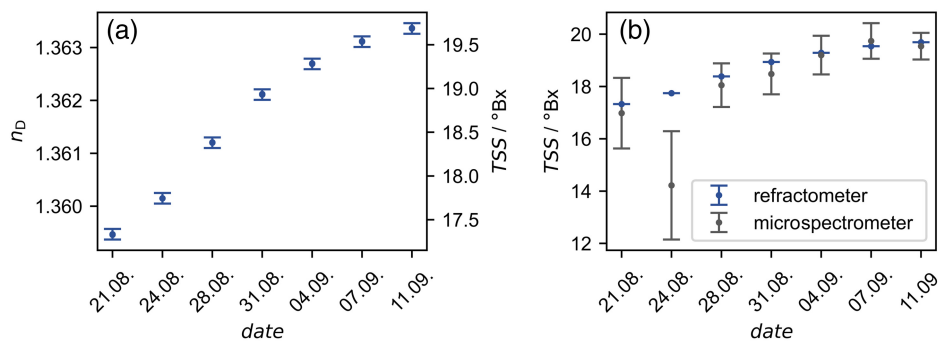

Fig. 9 Measurement of the amount of TSSs measured during a maturation period: (a) Reference values calculated from the refractive index of 20 mashed grape berries picked from the same vineyard the microspectrometer was evaluated. The error bars arise from the limited accuracy of the refractometer. (b) Microspectrometer measurements performed on grapes in the same vineyard can reproduce these values; the correlation coefficient of the reference values with the data obtained from the microspectrometer is 0.82 (excluding the outlier measured on 24.08).

However, two things are observed. First, the standard deviation decreased as the maturation proceeded. The reason for this lies in a higher inhomogeneity of the maturation at the start of the measurements: some berries are already colored, and others still are green, as seen in Fig. 8. Second, an outlier with a lower mean value and high standard deviation was measured on August 24, 2023. On that evening, exceptionally strong rain caused high water accumulation inside the grape bunches, leading to a higher variation of the measurement signals of the five microspectrometers. On the other days, there was no rain and no accumulation of water could be seen on the microspectrometer or the grape bunch.

6 Conclusions

We have demonstrated the design, fabrication, and characterization of a flexible microspectrometer suitable for continuous monitoring of the maturation process of grapes in the vineyard.

Further research needs to focus on the increase of the signal robustness. As also seen in the data presented in this paper, the measurement results currently strongly depend on the weather conditions in the vineyard. In the event of rain, optical conditions are changed, causing a signal distortion until the grape bunch is dry again. New generations of microspectrometers should be able to correct their results for different weather conditions.

Another aspect relevant to increased signal quality is the position of the sensor head with respect to the grape berry. The positioning has a large impact on the measured signal, confirming the results of the optical simulations. However, the position of the microspectrometer within the grape may also change during the maturation period. An approach to circumvent this limitation would be to add a position-sensing unit into the spectrometer head, which not only measures the distance to the grape berries but also the tilt with respect to the berry. Using this information, a correction factor could correct for position-related signal distortions.

Disclosures

The authors have no relevant conflicts of interest to disclose.

Code and Data Availability

The data supporting this study's findings are available upon reasonable request from the authors.

References

1. H. M. Oliveira et al., "An autonomous Internet of Things spectral sensing system for *in-situ* optical monitoring of grape ripening: design, characterization, and operation," *Comput. Electron. Agric.* **217**, 108599 (2024).
2. K. Ncama et al., "Application of Vis/NIR spectroscopy for predicting sweetness and flavour parameters of 'Valencia' orange (*Citrus sinensis*) and 'star ruby' grapefruit (*Citrus* x *paradisi* Macfad)," *J. Food Eng.* **193**, 86–94 (2017).
3. B. M. Nicola et al., "Nondestructive measurement of fruit and vegetable quality by means of NIR spectroscopy: a review," *Postharvest Biol. Technol.* **46**, 99–118 (2007).
4. R. Lu et al., "Measurement of optical properties of fruits and vegetables: a review," *Postharvest Biol. Technol.* **159**, 111003 (2020).
5. R. Civelli et al., "A simplified, light emitting diode (LED) based, modular system to be used for the rapid evaluation of fruit and vegetable quality: development and validation on dye solutions," *Sensors* **15**(9), 22705–22723 (2015).
6. J. L. Aleixandre-Tudo and W. D. Toit, *The Role of UV-Visible Spectroscopy for Phenolic Compounds Quantification in Winemaking*, pp. 200–204, IntechOpen, London (2018).

7. N. B. Ghozlen et al., "Non-destructive optical monitoring of grape maturation by proximal sensing," *Sensors* **10**, 10040–10068 (2010).

8. D. dos Santos Costa et al., "Development of predictive models for quality and maturation stage attributes of wine grapes using VIS-NIR reflectance spectroscopy," *Postharvest Biol. Technol.* **150**, 166–178 (2019).

9. G. Agati et al., "Assessment of anthocyanins in grape (*Vitis vinifera* L.) berries using a noninvasive chlorophyll fluorescence method," *J. Agric. Food. Chem.* **55**(4), 1053–1061 (2007).

10. G. Agati et al., "Potential of a multiparametric optical sensor for determining in situ the maturity components of red and white vitis vinifera wine grapes," *J. Agric. Food. Chem.* **61**, 12211–12218 (2013).

11. A. Pampuri et al., "Design of cost-effective LED based prototypes for the evaluation of grape (*Vitis vinifera* L.) ripeness," *Comput. Electron. Agric.* **189**, 106381 (2021).

12. L. Rocchi, L. Rustioni, and O. Failla, "Chlorophyll and carotenoid quantifications in white grape (*Vitis vinifera* L.) skins by reflectance spectroscopy," *VITIS J. Grapevine Res.* **55**(1), 11–16 (2016).

13. V. Giovenzana et al., "Wavelength selection with a view to a simplified handheld optical system to estimate grape ripeness," *Am. J. Enol. Viticult.* **65**(1), 117–123 (2013).

14. A. Ribera-Fonseca et al., "Assessment of technological maturity parameters and anthocyanins in berries of cv. Sangiovese (*Vitis vinifera* L.) by a portable vis/NIR device," *Sci. Horticult.* **209**, 229–235 (2016).

15. S. Jenne and H. Zappe, "Simulation of light interaction with seedless grapes," *J. Sci. Food Agric.* **103**, 57–63 (2022).

16. S. Jenne and H. Zappe, "Simulation of the optical properties of seedless grapes including Henyey-Greenstein scattering," in *3D Image Acquisit. and Disp.: Technol., Percept. and Appl.*, Optica, p. JTu2A. 8 (2022).

17. S. Prahl, "Scottprahl/IAD: forward and inverse radiative transport using the adding-doubling method," 2021, https://github.com/scottprahl/iad.

18. S. A. Prahl, M. J. C. van Gemert, and A. J. Welch, "Determining the optical properties of turbid media by using the adding–doubling method," *Appl. Opt.* **32**, 559 (1993).

19. D. Xie and W. Guo, "Measurement and calculation methods on absorption and scattering properties of turbid food in Vis/NIR range," *Food Bioprocess Technol.* **13**(2), 229–244 (2020).

20. B. C. Wilson and S. L. Jacques, "Optical reflectance and transmittance of tissues: principles and applications," *IEEE J. Quantum Electron.* **26**(12), 2186–2199 (1990).

21. J. Ordonez et al., "Thin films and microelectrode arrays for neuroprosthetics," *MRS Bull.* **37**(6), 590–598 (2012).

22. D. Ruh et al., "Stretchable optoelectronic circuits embedded in a polymer network," *Adv. Mater.* **26**(11), 1706–1710 (2013).

23. S. F. Price et al., "Cluster sun exposure and quercetin in pinot noir grapes and wine," *Am. J. Enol. Viticult.* **46**(2), 187–194 (1995).

24. S. Ustin et al., "Retrieval of foliar information about plant pigment systems from high resolution spectroscopy," *Remote Sens. Environ.* **113**(Suppl. 1), S67–S77 (2009).

25. R. Delgado-Pelayo, L. Gallardo-Guerrero, and D. Hornero-Méndez, "Chlorophyll and carotenoid pigments in the peel and flesh of commercial apple fruit varieties," *Food Res. Int.* **65**, 272–281 (2014).

26. "ICUMSA Specification and Standard SPS-3 Refractometry and Tables-Official; Tables A-F," Methods Book, ICUMSA, Berlin, Germany (2009).

Sophie Jenne received her BSc and MSc degrees in microsystems engineering from the University of Freiburg, Germany, in 2017 and 2020, respectively. Since 2020, she has worked as a PhD candidate at the Laboratory for Micro-optics in the same department. Her research interests include the development of tissue phantoms and flexible microspectrometers for biomedical and agricultural applications.

Alessio Tugnolo is a research fellow at Università degli Studi di Milano. He received his BSc, MSc, and European PhD in food systems in 2022 from the same university. His research activities focus on the application of nondestructive spectroscopic techniques and the design of optical sensors combined with the multivariate statistical approach for the safety and quality assessment of agri-food products.

Hugo M. Oliveira is a staff researcher at the International Iberian Nanotechnology Laboratory. He received his BSc and MSc from the University of Porto. He also received the European PhD in analytical chemistry from the same university. He worked at the University of Hawaii and University of Porto before joining INL in 2016. His current research interests are focused on the development of integrated sensing solutions for agri-food and environment.

Hans Zappe is a professor of micro-optics at the University of Freiburg, Germany. He earned his BSc and MSc degrees from MIT in 1983 and his PhD from the University of California, Berkeley in 1989, all in electrical engineering. He worked at IBM (USA), the Fraunhofer Institute for Applied Solid State Physics (Germany), and the Centre Suisse d'Electronique et de Microtechnique (Switzerland) before joining the Department of Microsystems Engineering at the University of Freiburg in 2000. He is a fellow of SPIE, OSA, and IOP.